nature chemistry

SUPPLEMENTARY INFORMATION

DOI: 10.1038/NCHEM.2875

In the format provided by the authors and unedited.

Self-assembly of polyhedral metal–organic framework particles into three-dimensional ordered superstructures

Civan Avci, Inhar Imaz, Arnau Carné-Sánchez, Jose Angel Pariente, Nikos Tasios, Javier Pérez-Carvajal, Maria Isabel Alonso, Alvaro Blanco, Marjolein Dijkstra, Cefe Lopez, and Daniel Maspoch

INDEX

Supplementary Section 1: Characterisation

A. Materials. All chemical reagents and solvents were purchased from Sigma Aldrich and used as received without further purification. Deionised (DI) H_2O was obtained from a Milli-Q water purification system.

B. Instrumentation. Field-emission scanning electron microscopy (FE-SEM) images were collected on a scanning electron microscope (FEI Magellan 400L XHR) at an acceleration voltage of 1.0 kV, using conductive carbon tape. The size of crystals was calculated from FE-SEM images by averaging the distance of a {100} facet to its opposite {100} facet of 200 particles from images of different areas of the same samples. X-ray powder diffraction (XRPD) measurements were made on an X'Pert PRO MPD diffractometer (Panalytical), with λ_{Cu} = 1.5406 Å. The surface charge of MOF particles (expressed as zeta potential (ζ)) was measured using a Malvern Zetasizer, (Malvern Instruments, UK). Volumetric N_2 sorption measurements were collected at 77 K using an ASAP 2020 HD gas adsorption system (Micromeritics). The reflectance spectra were taken with a Hyperion 2000 FT-IR microscope coupled to a Vertex 80 Spectrometer (both from Bruker) with a 15× Schwarzschild standard objective, tungsten lamp (in the Vertex 80) and a Si-diode detector. Thermogravimetric analysis (TGA) measurements were performed under a nitrogen flow heating from 30ºC to 700ºC at a heating rate of 10ºC/min using a Pyris 8000 Thermo Gravimetric Analyzer. Ellipsometry measurements were made on a GES5E rotating polariser ellipsometer (SOPRALAB) at six angles of incidence: from 45º to 70º (at intervals of 5º) in a spectral range from *ca.* 230 nm to 1030 nm. The effective refractive index was evaluated for wavelengths that did not fulfil the Bragg condition. Since Bragg-like reflection features in the investigated self-assembled superstructure appeared in the wavelength range below 580 nm, we restricted the analysis of ellipsometry data to longer wavelengths (from 620 nm to 1030 nm). Moreover, as the sample surface was obviously rough, we included the roughness layer to model the ellipsometry data in a standard way. In order to compare the results to those from reflectometry, we considered a constant isotropic effective refractive index. The best-fit results for the as-made and activated photonic crystals exhibited constant refractive indexes of n = 1.43 and 1.40, respectively. The roughness-layer thicknesses obtained from the fits were 64 ± 2 nm and 87 ± 8 nm in fair agreement with the step height (w) present in the stacking.

C. Guest sorption measurements. In order to track *in-situ* the change in band gap of the photonic crystal upon water evacuation, and alcohol and water sorption, we designed and assembled a custom vapour chamber. For the water evacuation, the as-prepared photonic crystal made from 210 nm TRD ZIF-8 particles was first activated in an oven at 260 ^{o}C for 30 min, and then placed in a glass chamber that comprised a glass cuvette (used for UV-Vis spectroscopy) and a rubber sealing. A spectrum was collected from the activated sample. Then, the alcohol of interest or water was put in a separate bottle that had two plastic tubes on its cap. One end of the first tube was dipped into the alcohol/water and the other end was connected to the gas source that was used for bubbling the alcohol/water. The second tube in the bottle was used for transferring the alcohol/water vapours to the sample chamber. The alcohol/water vapours passed through the sample chamber by continuous air bubbling of the alcohol/water. In order to complete the vapour flow, we pierced the rubber sealing of the sample chamber with an empty needle. For the adsorption, the bubbling continued until (depending on the alcohol) the photonic superstructure did not exhibit any further shift in the band gap. Desorption was performed by purging with air the chamber until the band gap shifted back to its initial position of 522 nm. Additional heating (120 ^{o}C for 10 min) in the oven was necessary in the cases of *i*-PrOH and *n*-BuOH, as the desorption of each was relatively slower than that of MeOH or EtOH.

Supplementary Figure 1. Simulated (black) and synthesised XRPD patterns of ZIF-8 particles of different sizes: 178 ± 8 nm (blue); 193 ± 8 nm (green); 210 ± 10 nm (red); and 227 ± 10 nm (purple).

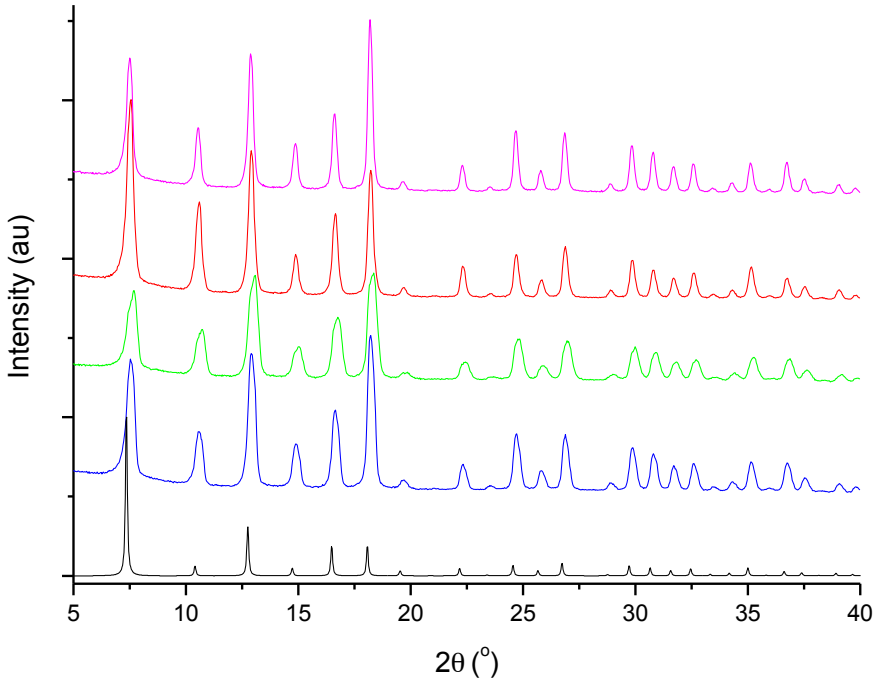

Supplementary Figure 2. Representative N_2 sorption isotherm of the synthesised ZIF-8 with a particle size of 210 ± 10 nm.

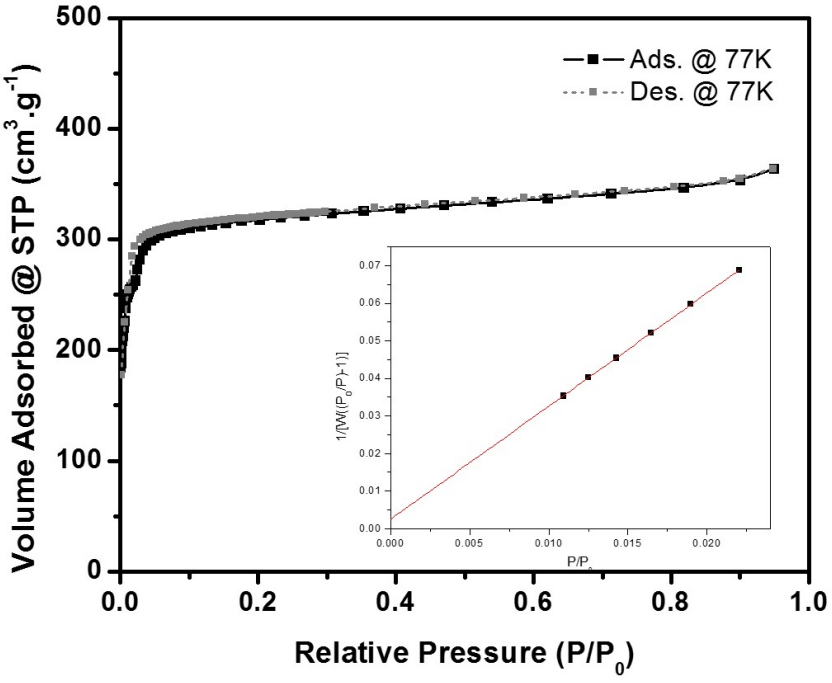

Surface area = 1154 m²/g

Slope = 3.013

Intercept = 2.469e-03

Correlation coefficient, r = 0.999954

C constant = 1221

Pore volume = 0.50 cm^3/g

Supplementary Figure 3. Representative FE-SEM images of well-ordered superstructures self-assembled from ZIF particles of different sizes: a) 178 ± 8 nm; b) 193 ± 8 nm; and c) 227 ± 10 nm. Scale bars: 5 μm (left column) and 2 μm (right column).

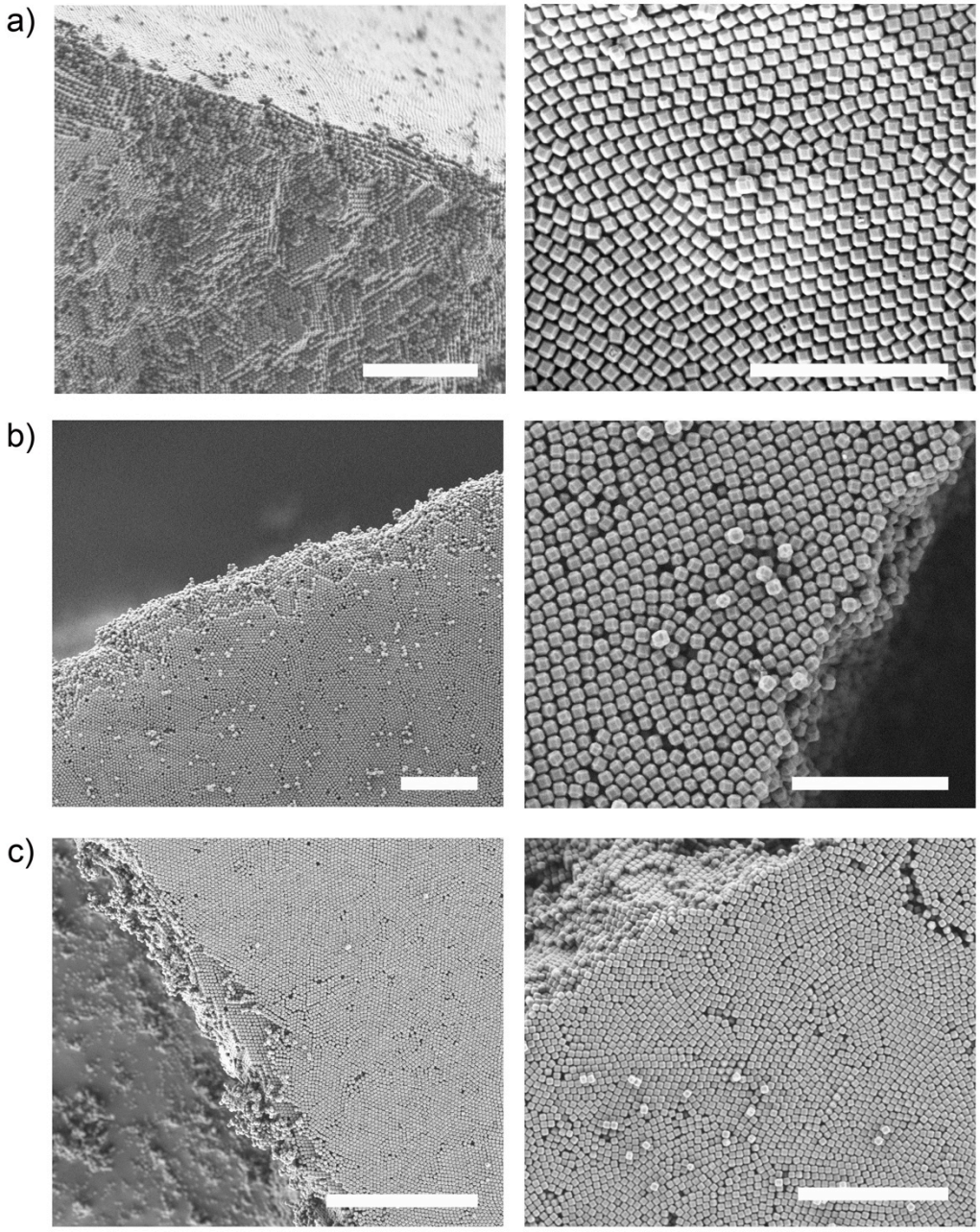

Supplementary Figure 4. Representative FE-SEM images of the self-assembled superstructures obtained using different techniques: a) evaporation at RT; b) evaporation at 100 ^{o}C; c) spin coating; d) dip coating; and e) vertical deposition. Scale bars: 10 μm (left column) and 5 μm (right column).

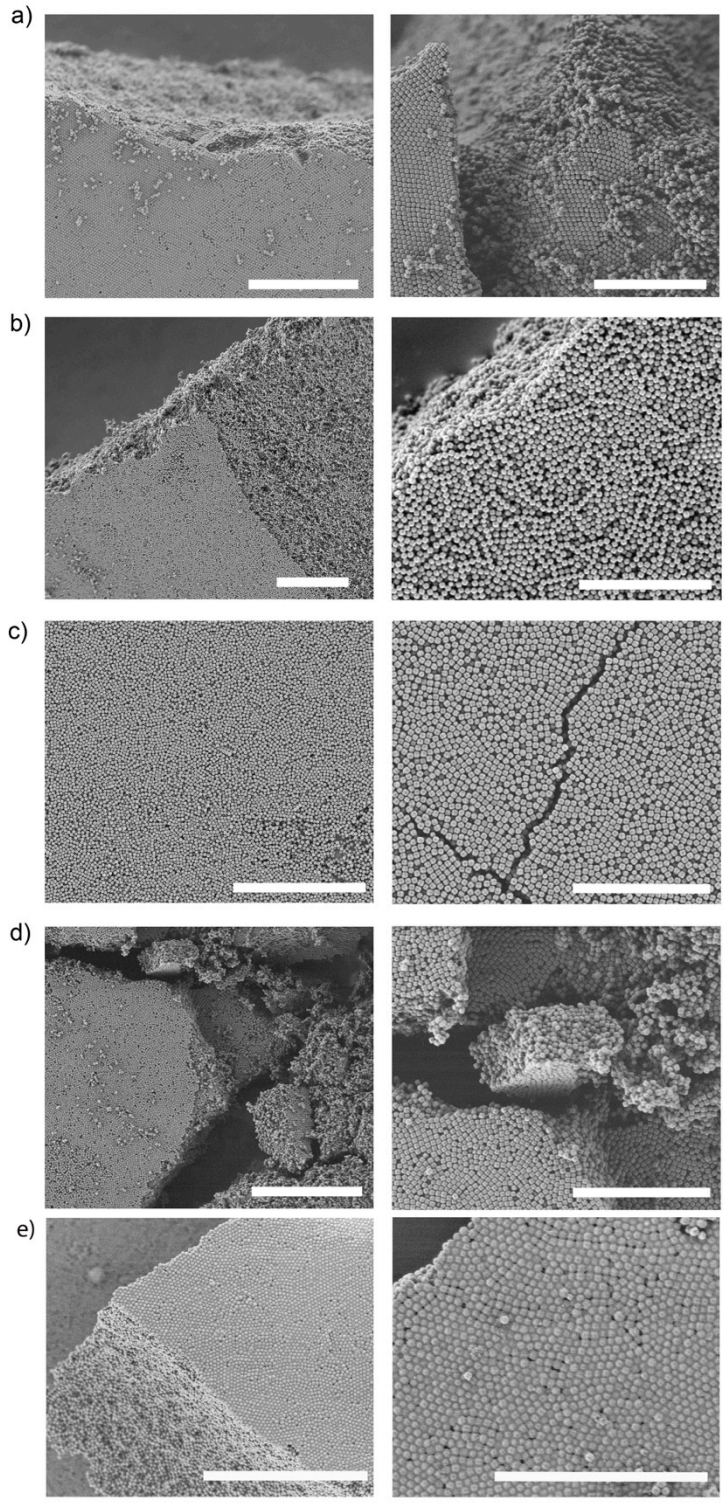

Supplementary Figure 5. a) Photograph of the self-assembled superstructures resulting from the centrifugation of an aqueous colloidal solution of ZIF-8 particles of different sizes. Note here the opalescence visible to the naked eye, which confirms a certain degree of ordering in these structures. b) Representative FE-SEM image of self-assembled superstructures resulting from this centrifugation step. Scale bars: 1 μm (b, left) and 5 μm (b, right).

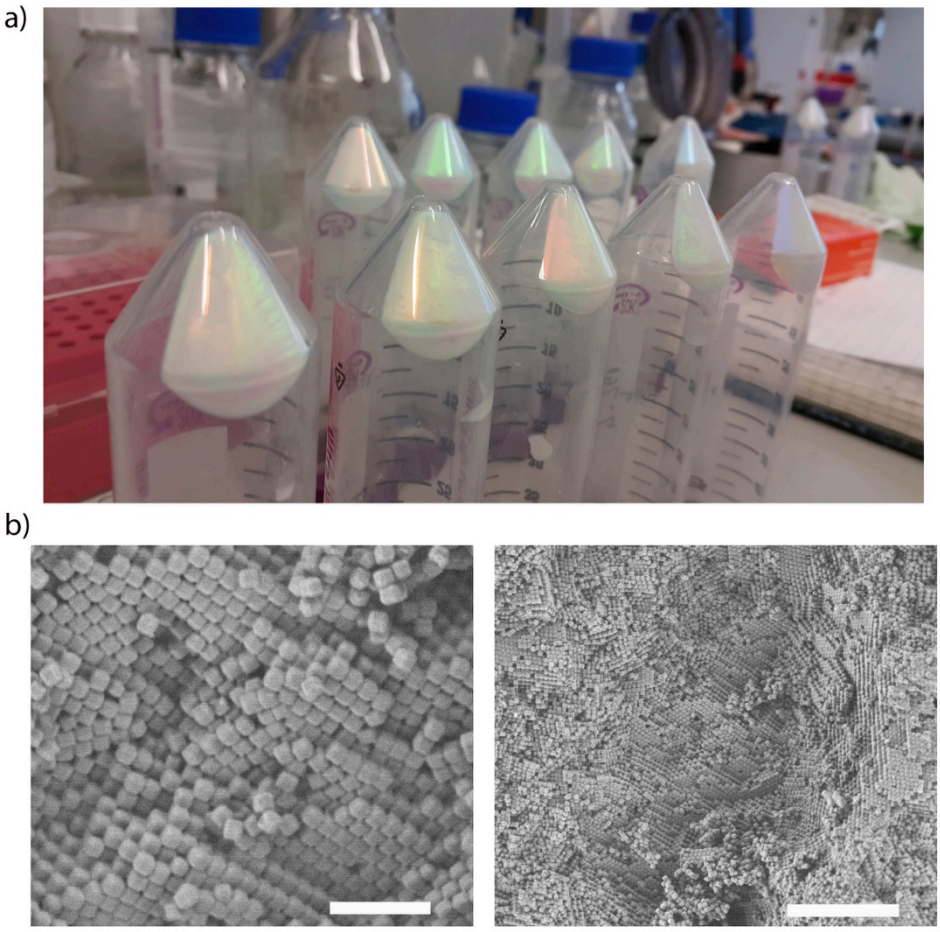

Supplementary Figure 6. Optical reflectance at θ = 0º for the photonic crystals made of TRD ZIF-8 particles of different sizes: 178 ± 8 nm (blue); 193 ± 8 nm (green); 210 ± 10 nm (yellow); and 227 ± 10 nm (red).

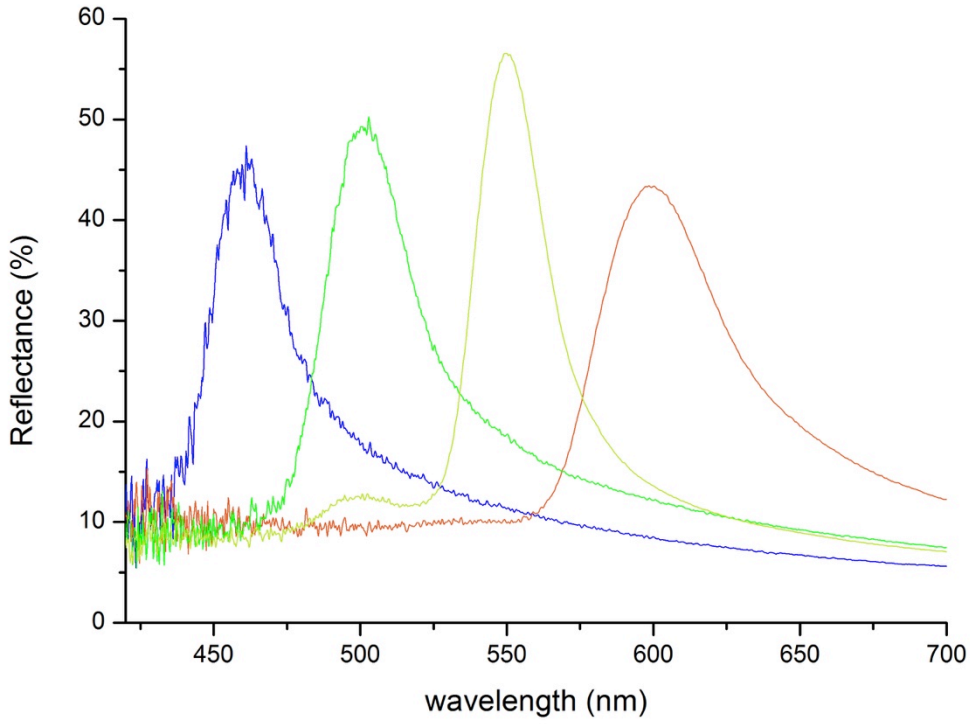

Supplementary Figure 7. Measured ellipsometric magnitudes (symbols) at several angles of incidence φ for the as-made photonic crystal made of TRD ZIF-8 particles sized 210 ± 10 nm, compared to the fittings, from which a refractive index *n* of 1.432 was deduced. Only the measured wavelength range (620 nm to 1030 nm) in which the material can be considered an effective medium is shown. (a) tan ψ and (b) cos Δ. The roughness-layer thickness obtained from the fitting was 64 ± 2 nm.

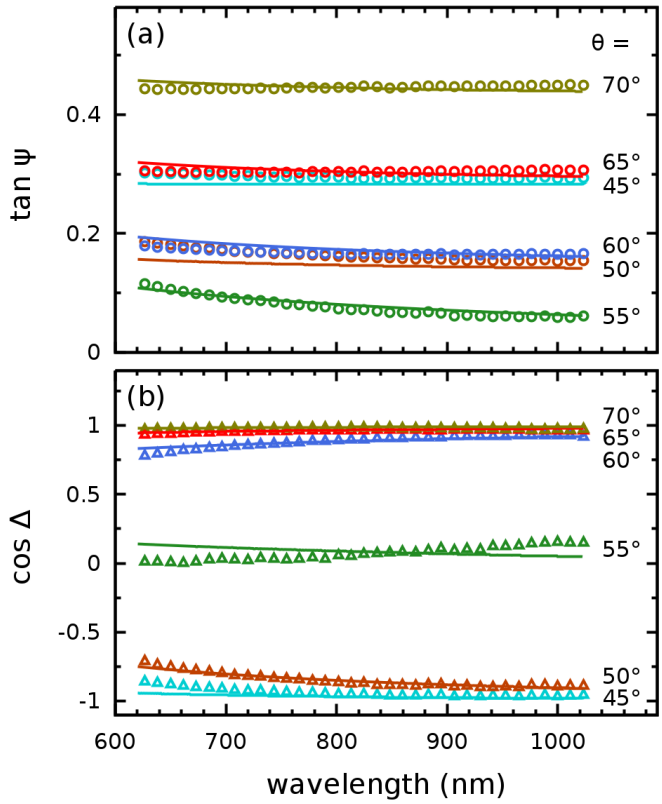

Supplementary Figure 8. Linear relation (r = 0.998) between the edge length *x* and the chamfer *w* of the different synthesised TRD ZIF-8 particles.

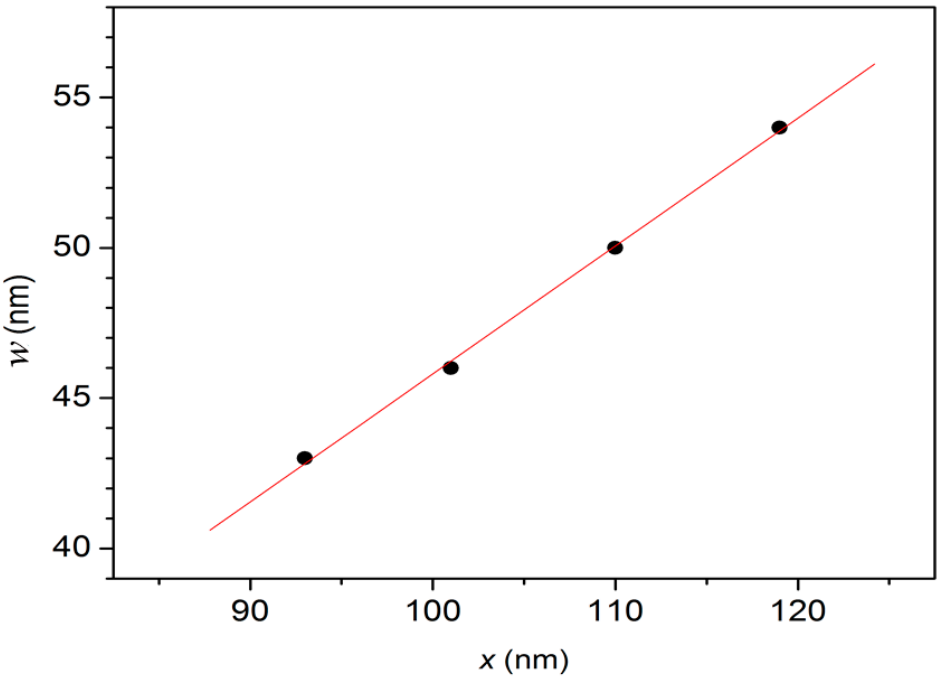

Supplementary Figure 9. TGA of the as-made (red) and activated (blue) photonic crystal made of TRD ZIF-8 particles sized 210 ± 10 nm.

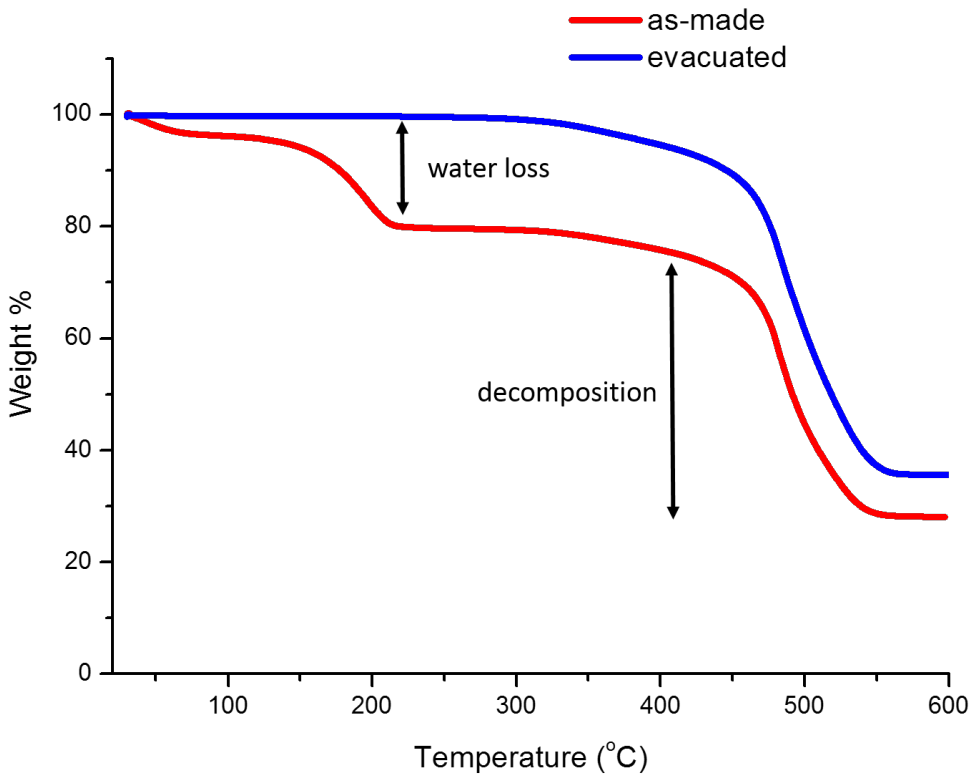

Supplementary Figure 10. (a,b) FE-SEM images of the activated photonic crystal made of TRD ZIF-8 particles sized 210 ± 10 nm. (c,d) FE-SEM images of the photonic crystal after alcohol adsorption experiments. Scale bars: 5 μm (a,c,d) and 3 μm (b).

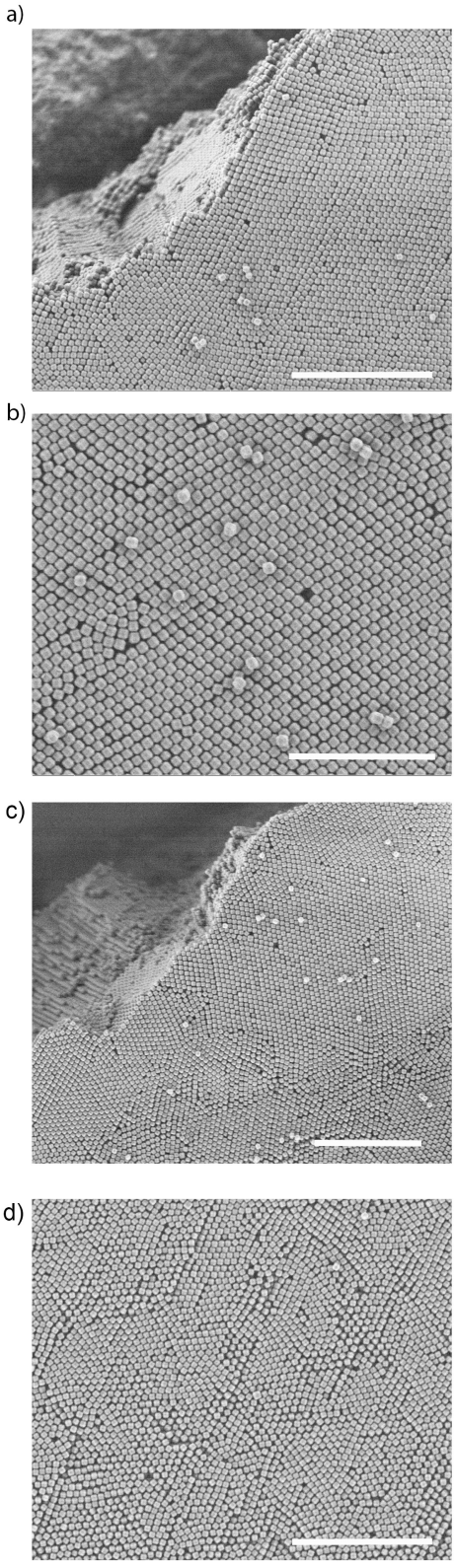

Supplementary Figure 11. Representative N_2 sorption isotherm of the photonic crystal made of TRD ZIF-8 particles sized 210 ± 10 nm.

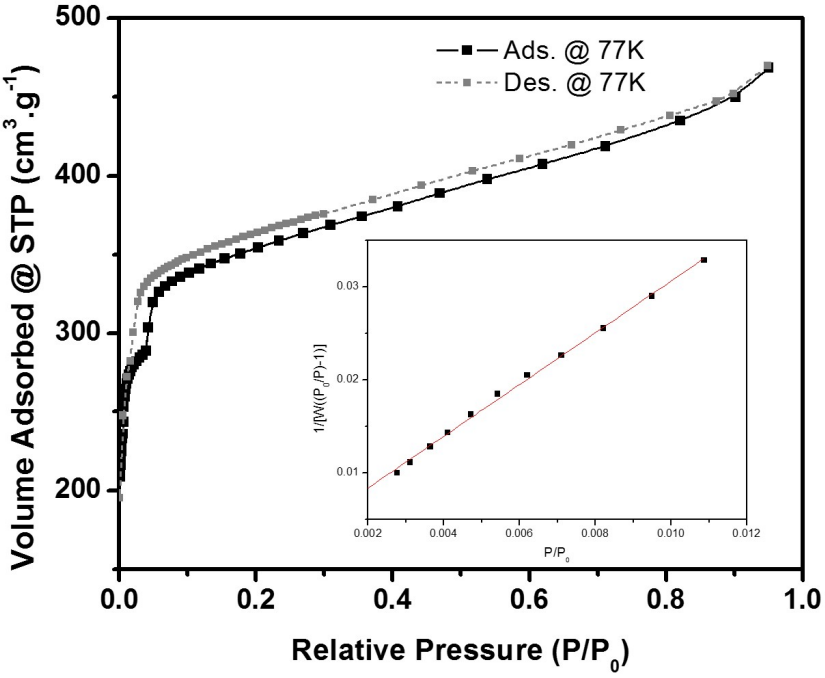

Surface area = 1250 m²/g

Slope = 2.784

Intercept = 2.788e-03

Correlation coefficient, r = 0.9989

C constant = 999

Pore volume = 0.57 cm^3/g

Supplementary Figure 12. Optical reflectance at θ = 0º for the as-made and activated photonic crystal made of TRD ZIF-8 particles sized 210 ± 10 nm.

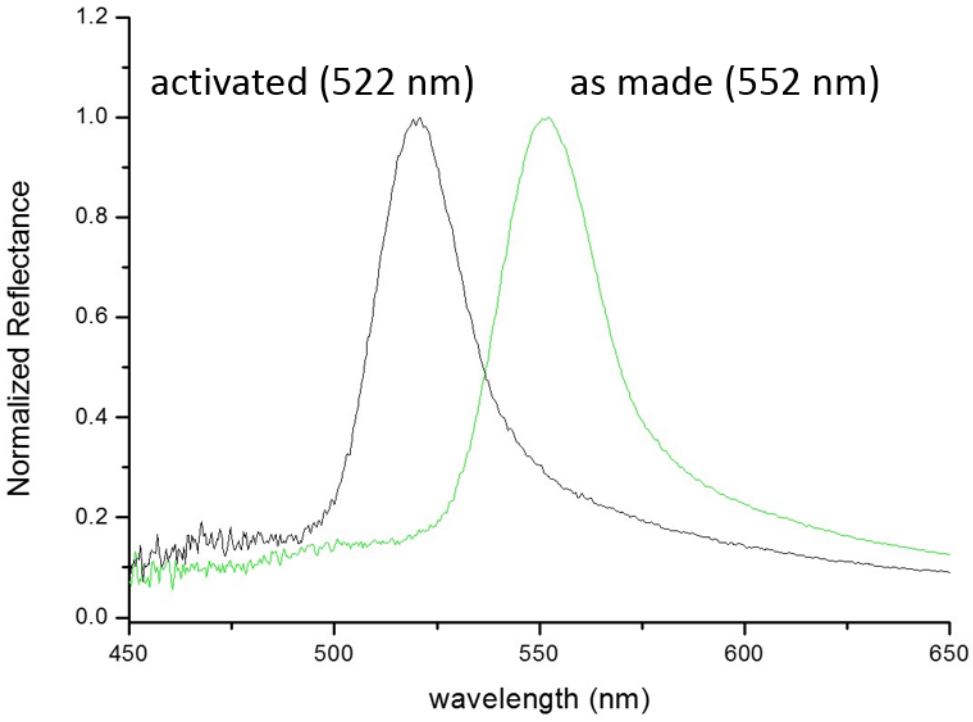

Supplementary Figure 13. Optical reflectance at θ = 0º for the photonic crystal made of TRD ZIF-8 particles sized 210 ± 10 nm: as-made (light green), activated (black), and after exposure of the latter to MeOH (red), EtOH (blue), *i*-PrOH (violet), or *n*-BuOH (dark green).

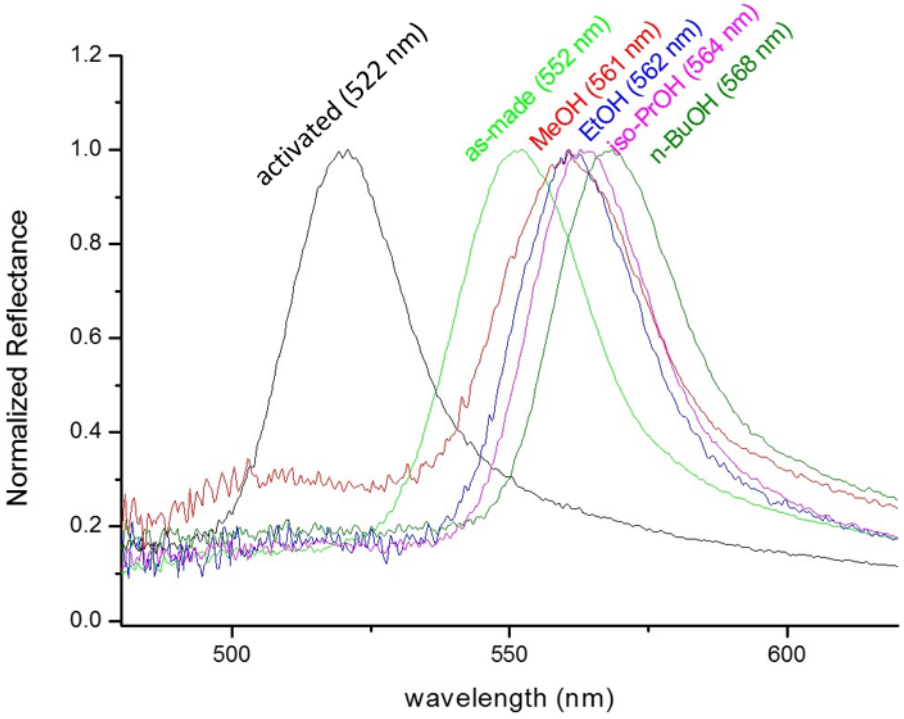

Supplementary Figure 14. Optical reflectance at θ = 0º for the photonic crystal made of TRD ZIF-8 particles sized 210 ± 10 nm: activated (black), and after exposure to water (blue).

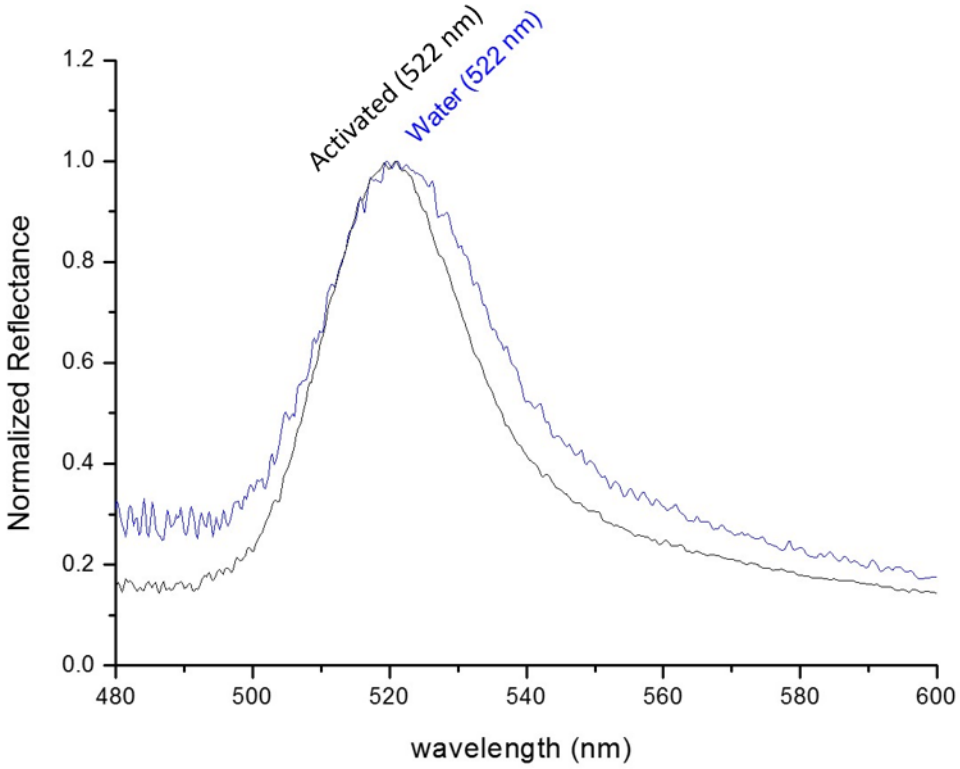

Supplementary Figure 15. Alcohol and water sorption isotherms of the photonic crystal made of TRD ZIF-8 particles sized 210 ± 10 nm.

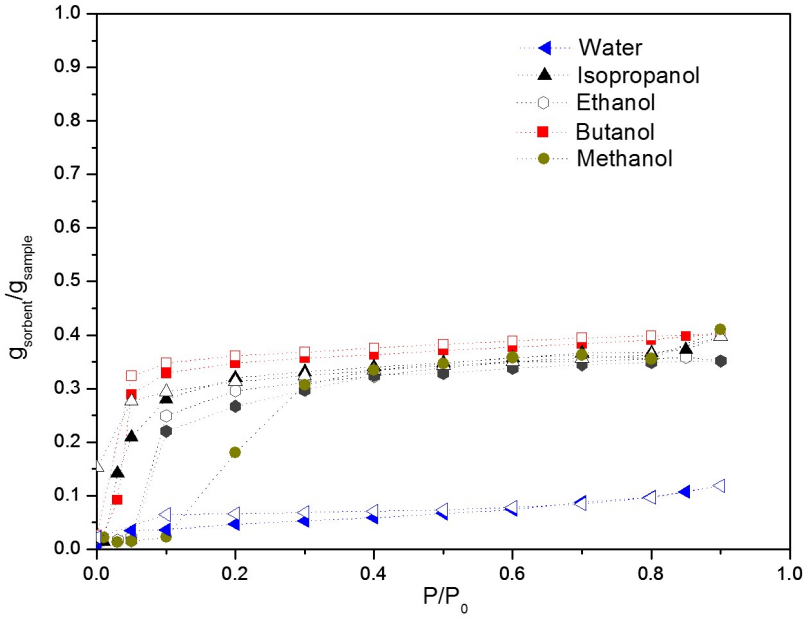

Supplementary Figure 16. Measured ellipsometric quantities (symbols) at several angles of incidence φ for the activated photonic crystal made of TRD ZIF-8 particles sized 210 ± 10 nm compared to the fittings from which the refractive index n = 1.40 was deduced for the activated sample. Only the measured wavelength range (620 nm to 1030 nm) in which the material can be considered an effective medium is shown. (a) tan ψ, (b) cos Δ. The roughness-layer thickness obtained from these fits was 87 ± 8 nm.

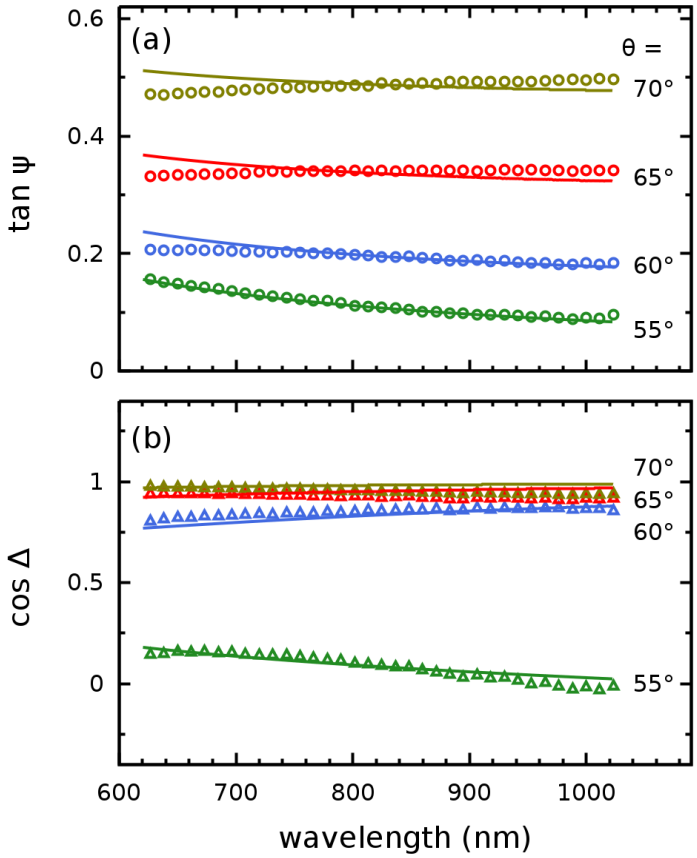

Supplementary Figure 17. Representative FE-SEM images of (a,b) TRD ZIF-8 particles with t = 0.57; (e,f) TRD ZIF-8 particles with t = 0.38; (i,j) RD ZIF-8 particles; and (m,n) octahedral UiO-66 particles. Scale bars: 3 μm (a,e,i,m) or 500 nm (b,f,j,n). Size-distribution histograms of (c) TRD ZIF-8 particles with t = 0.57; (g) TRD ZIF-8 particles with t = 0.38; (k) RD ZIF-8 particles; and (o) octahedral UiO-66 particles. Simulated (black) and synthesised XRPD patterns of (d) TRD ZIF-8 particles with t = 0.57; (h) TRD ZIF-8 particles with t = 0.38; (l) RD ZIF-8 particles; and (p) octahedral UiO-66 particles.

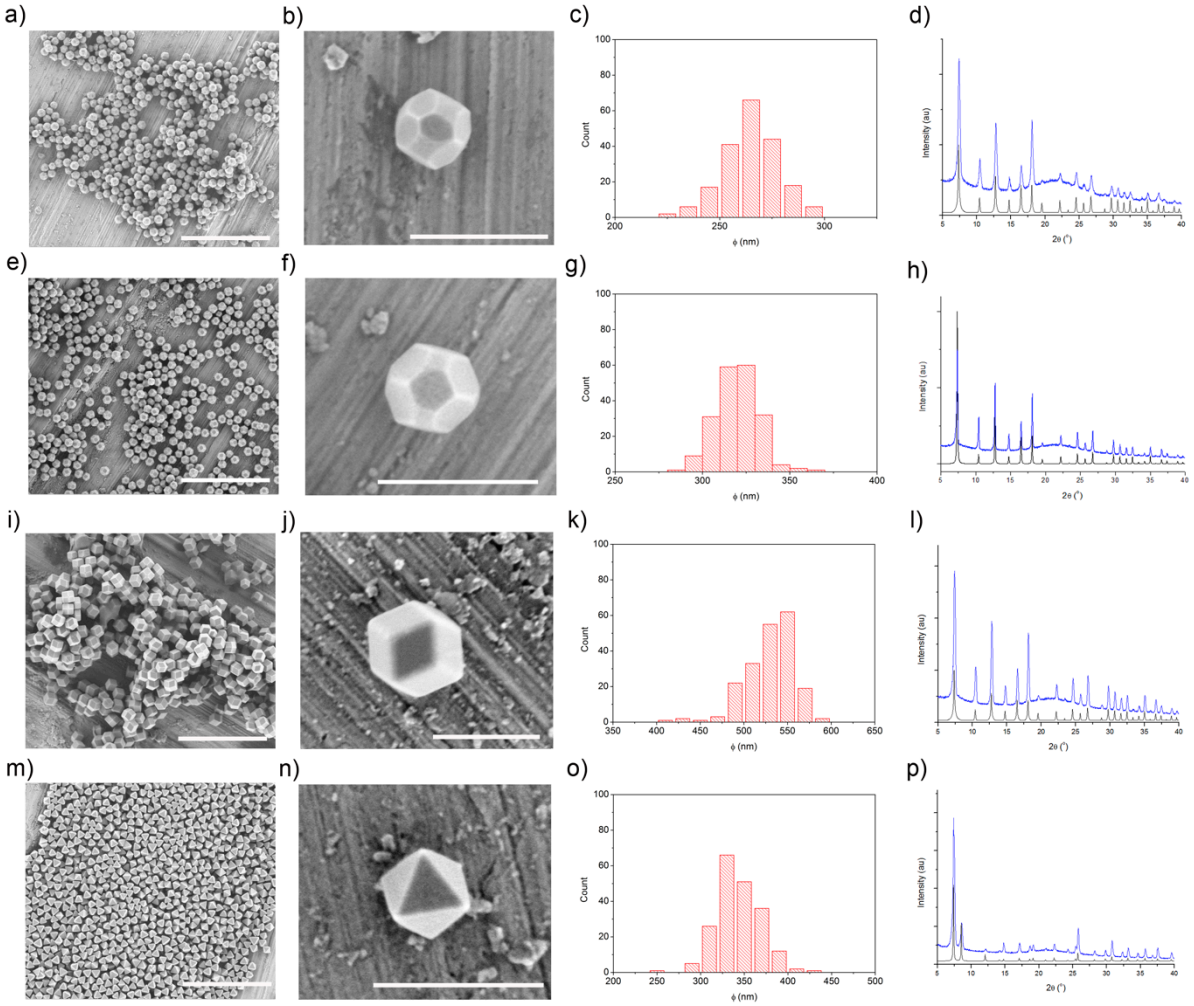

Supplementary Figure 18. Additional FE-SEM images of the self-assembled superstructures made of (a,b) TRD ZIF-8 particles with $t = 0.57$; (c,d) TRD ZIF-8 particles with $t = 0.38$; and (i,f) octahedral UiO-66 particles. Scale bars: 10 μm (c), 3 μm (a,e), 2 μm (b), and 1 μm (d,f).

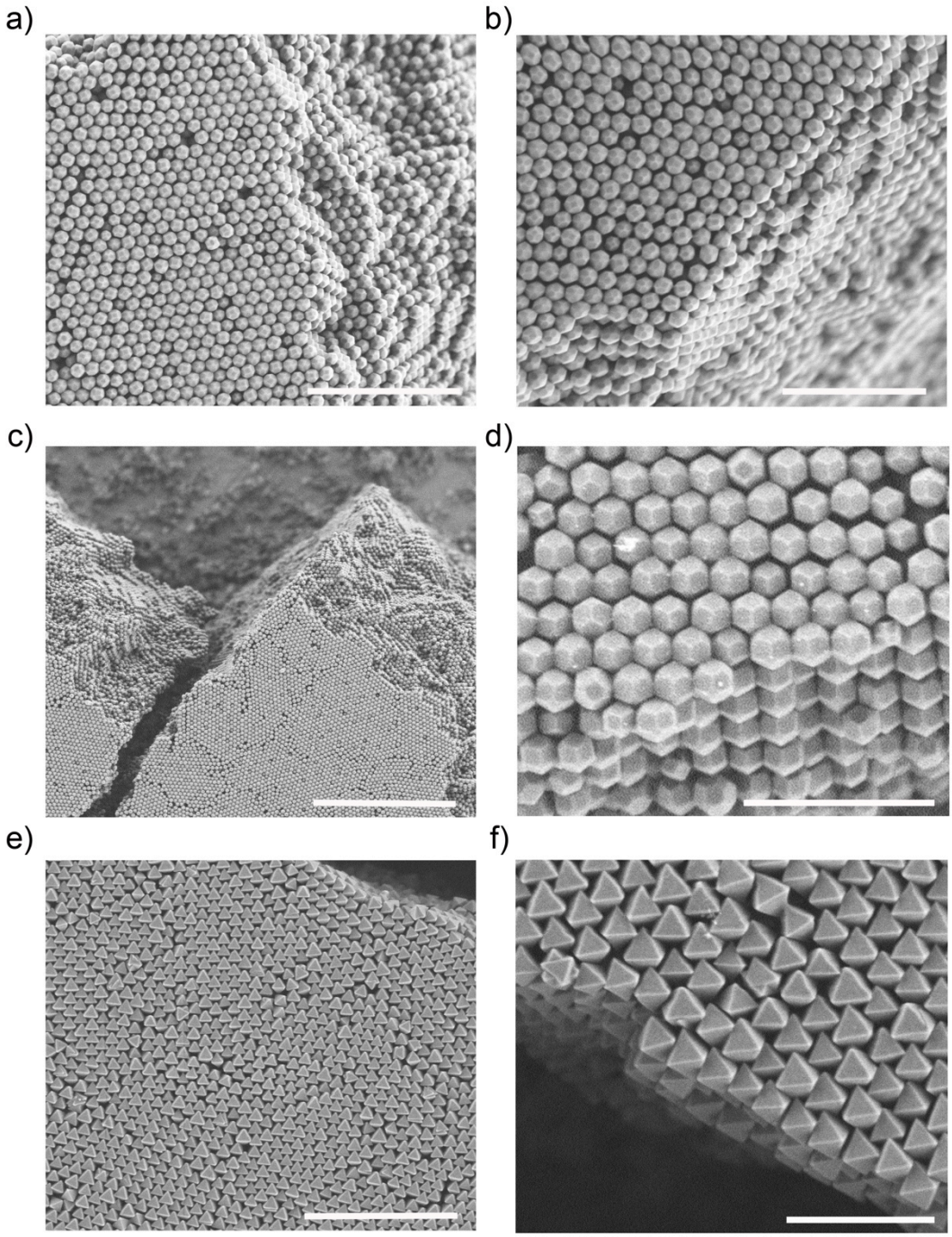

Supplementary Figure 19. N_2 sorption isotherm of the plastic crystal made of TRD ZIF-8 particles with $t = 0.57$.

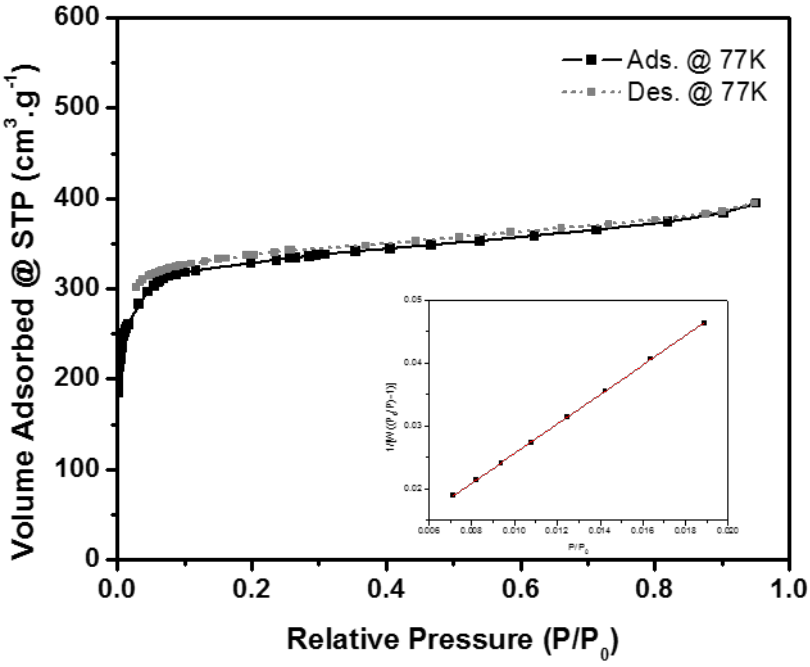

Surface area = 1201 m²/g

Slope = 2.343

Intercept = 2.15e-03

Correlation coefficient, r = 0.9999

C constant = 1086

Pore volume = 0.52 cm^3/g

Supplementary Figure 20. N_2 sorption isotherm of the ordered superstructure made of RD ZIF-8 particles.

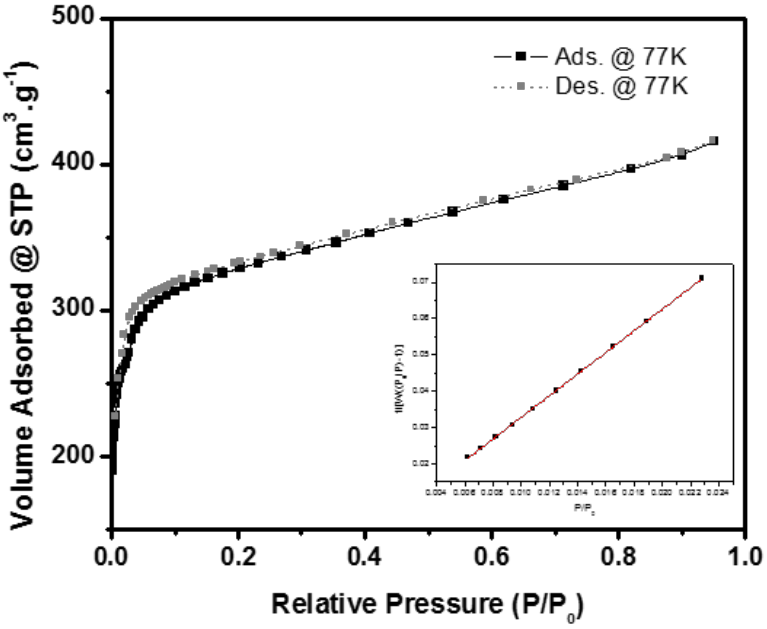

Surface area = 1168 m²/g

Slope = 2.977

Intercept = 2.788e-03

Correlation coefficient, r = 0.9999

C constant = 990

Pore volume = 0.53 cm^3/g

Supplementary Figure 21. N_2 sorption isotherm of the ordered superstructure made of octahedral UiO-66 particles.

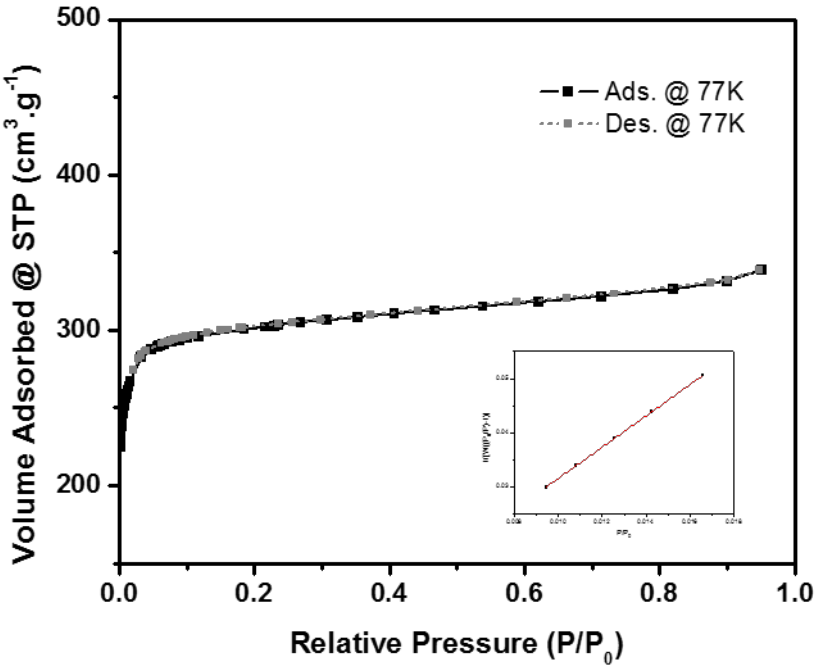

Surface area = 1240 m²/g

Slope = 2.827

Intercept = 0.033

Correlation coefficient, r = 0.9999

C constant = 835

Pore volume = 0.47 cm^3/g

Supplementary Section 2: Determination of the Effective Refractive Indexes and Shifts of the Photonic Band Gaps

A. Effective refractive index of the dense ZIF-8 framework

In order to calculate the theoretical shifts of the band gap of the photonic crystal made of TRD ZIF-8 particles (size: 210 ± 10 nm) due to the inclusion of guest molecules, we first determined the effective refractive index of the dense ZIF-8 framework (n_{fram}) without considering the pores. To do this, we determined the effective refractive index of the activated photonic crystal using the Bragg-Snell law (Equation 1):

$$\lambda_{activated} = 2dn_{activated} \quad (1)$$

where $\lambda_{activated}$ is 522 nm (as measured from the reflectance spectra; Figure S8) and d is the interplanar distance of 184 nm. The effective refractive index $n_{activated}$, which corresponds to the photonic crystal free of water, was found to be 1.42. This value is in good agreement with the value (1.40) obtained by spectroscopic ellipsometry performed on the activated photonic crystal self-assembled from 210-nm TRD ZIF-8 particles (Supplementary Fig. S16).

We then calculated the occupancy of the interparticle voids in the photonic crystal according to Equation 2:

$$V_{void} = 1 - f \quad (2)$$

where f is the packing fraction of the rhombohedral packing (f = 0.86) and V_{void} is 0.14. Owing to their porous nature, ZIF-8 crystals comprise the solid framework and the micropores. The theoretical micropore volume of ZIF-8 is 0.54 cm^3/g, which corresponds to a volumetric occupancy of 50%. From the N_2 sorption isotherm of the photonic crystal, we measured a pore volume of 0.57 cm^3/g, which is quite close to this theoretical value. Accordingly, in the photonic crystal the fraction of volume that corresponds to the dense ZIF-

8 framework (V_{fram}) is 0.43; that which corresponds to accessible micropores (V_{micro}), is also 0.43; and that representing interparticle voids (V_{void}), is 0.14. Combining the volume fractions for the micropores and the interparticle voids, and considering then that the resulting space is filled with air, yields an air-volume fraction (V_{air}) of 0.57 in the photonic crystal.

The effective refractive index of the activated photonic crystal can also be calculated according to Equation 3:

$$n_{activated} = \sqrt{V_{fram} n_{fram}^2 + V_{air} n_{air}^2} \quad (3)$$

where n_{air} is 1.00.[1] From this equation, the effective refractive index of the dense ZIF-8 framework (n_{fram}) is calculated to be 1.83.

B. Effective refractive index of the as-made (water-loaded) photonic crystal

The TGA of the as-made photonic crystal shows that it contains 21% (w/w) water (Figure S8). Considering that the density of ZIF-8 is 0.925 g/cm^3,[2] this amount of water corresponds to a volume fraction of water (V_{water}) of 0.21 in the total photonic crystal. Therefore, the as-made photonic crystal is composed of the dense ZIF-8 framework (V_{fram} = 0.43, n_{fram} = 1.83), water (V_{water} = 0.21, n_{water} = 1.33)[3] and air (V_{air} = 0.36, n_{air} = 1.00). From Equation 4, the effective refractive index of the as-made photonic crystal is calculated to be 1.47 (see also Table S1).

$$n_{as\text{-}made} = \sqrt{V_{fram} n_{fram}^2 + V_{H2O} n_{H2O}^2 + V_{air} n_{air}^2} \quad (4)$$

C. Shifts in the band gaps of the photonic crystals upon exposure to alcohols

The alcohol sorption isotherms measured for the photonic crystal (Figure S12) revealed that it can take up to 35% (w/w) of MeOH, EtOH, or *i*-PrOH, or up to 38% (w/w) of *n*-BuOH. These uptake values are equivalent to a volume fraction of 0.35 for MeOH, EtOH, and *i*-PrOH (V_{MeOH}, V_{EtOH} and $V_{i\text{-PrOH}}$), or 0.37 for *n*-BuOH ($V_{n\text{-BuOH}}$). With these values, the micropore filling of ZIF-8 particles is 81% for MeOH, EtOH, or *i*-PrOH, or 86% for *n*-BuOH. Using Equation 4, but substituting the water molecules with the corresponding alcohol molecules, the effective refractive indexes of the photonic crystal upon exposure to each alcohol is calculated to be: 1.51 for MeOH; 1.52 for EtOH; 1.53 for *i*-PrOH; and 1.54 for *n*-BuOH. The expected band gaps can then be calculated using the Bragg-Snell law. The obtained values are 556 nm for MeOH, 559 nm for EtOH, 561 nm for *i*-PrOH, and 567 nm for *n*-BuOH. These results and the experimental ones are summarised together in Table S1.

Supplementary Table 1: Experimental and calculated refractive indices and band gaps of the as-made photonic crystal (particle size: 210 ± 10 nm) before evacuation and subsequent exposure to different alcohols.

Guest molecule	Refractive index of guest molecule n_{guest}	Pore filling of the guest molecule (%)	Experimental refractive index n_{exp} [§]	Calculated refractive index n_{cal} *	Experimental band gap λ_c [††] (nm)	Calculated band gap λ_c ** (nm)
Water	1.33	49 [†]	1.49	1.47	552	543
Methanol	1.33[4]	81 [‡]	1.52	1.51	561	556
Ethanol	1.36[4]	81 [‡]	1.53	1.52	562	559
isopropanol	1.38[4]	81 [‡]	1.53	1.53	564	561
n-Butanol	1.40[4]	86 [‡]	1.54	1.54	568	567

[†] Measured from TGA

[‡] Measured from sorption isotherms

[§] Measured from the slope of the interplanar distance vs. the experimental band-gap plot

* Calculated using the equation $n_{eff} = \sqrt{V_{fram}n_{fram}^2 + V_{guest}n_{guest}^2 + V_{air}n_{air}^2}$.

[††] Measured from UV-Visible reflectance spectra

** Calculated using the Bragg-Snell law

References

1. Ciddor, P. E. Refractive index of air: new equations for the visible and near infrared. *Appl. Opt.* **35,** 1566–1573 (1996).
2. Radhakrishnan, D. & Narayana, Effect of pore occupancy on the acoustic properties of zeolitic imidazolate framework (ZIF)-8: A Brillouin spectroscopic study at ambient and low temperatures. *J. Chem. Phys.* **143,** 234703 (2015).
3. Hale, G. M. & Querry, M. R. Optical constants of water in the 200-nm to 200-µm wavelength region. *Appl. Opt.* **12,** 555–563 (1973).
4. O'Brien, R. N. & Quon, D. Refractive index of some alcohols and saturated hydrocarbons at 6328 A. *J. Chem. Eng. Data* **13,** 517 (1968).